

Plasma Sci. Technol. **24** (2022) 045503 (9pp) https://doi.org/10.1088/2058-6272/ac496e

In situ quantification of NO synthesis in a warm air glow discharge by WMS-based Mid-IR QCL absorption spectroscopy

Chuanqi WANG (汪传奇), **Junjie QIAO** (乔俊杰), **Yijia SONG** (宋一嘉), **Qi YANG** (杨琦), **Dazhi WANG** (王大智), **Qingyuan ZHANG** (张清源), **Zhan SHU** (舒展) **and Qing XIONG** (熊青)*

State Key Laboratory of Power Transmission Equipment & System Security and New Technology, Chongqing University, Chongqing 400044, People's Republic of China

E-mail: qingxiong@cqu.edu.cn

Received 3 November 2021, revised 4 January 2022
Accepted for publication 7 January 2022
Published 4 April 2022

Abstract

Nitric oxide (NO) is one of the most crucial products in the plasma-based nitrogen fixation process. In this work, *in situ* measurements were performed for quantifying the NO synthesis spatially in a warm air glow discharge, through the method of Mid-infrared quantum cascade laser absorption spectroscopy (QCL-AS). Two ro-vibrational transitions at 1900.076 cm^{-1} and 1900.517 cm^{-1} of the ground-state NO(X) were probed sensitively by the help of the wavelength modulation spectroscopy (WMS) approach to increase the signal/noise (S/N) level. The results show a decline trend of NO synthesis rate along the discharge channel from the cathode to the anode. However, from the point of energy efficiency, the cathode region is of significantly low energy efficiency of NO production. Severe disproportionality was found for the high energy consumption but low NO production in the region of cathode area, compared to that in the positive column zone. Further analysis demonstrates the high energy cost of NO production in the cathode region, is ascribed to the extremely high reduced electric field E/N therein not selectively preferable for the processes of vibrational excitation or dissociation of N_2 and O_2 molecules. This drags down the overall energy efficiency of NO synthesis by this typical warm air glow discharge, particularly for the ones with short electrode gaps. Limitations of further improving the energy cost of NO synthesis by variations of the discharge operation conditions, such as discharge current or airflow rate, imply other effective manners able to tune the energy delivery selectively to the NO formation process, are sorely needed.

Supplementary material for this article is available online

Keywords: nitric oxide, QCL absorption spectroscopy, WMS, energy efficiency, warm air discharge

(Some figures may appear in colour only in the online journal)

1. Introduction

As nitrogen compounds play important roles for live on Earth, the process of nitrogen fixation in which nitrogen-containing compounds are synthesized from air or air-containing gas mixtures, is of a particular importance. The Haber-Bosch process is known to be the most commonly applied technology for nitrogen fixation in industry at the moment, which uses N_2 and H_2 to catalyze the formation of NH_3 at high temperature and high pressure [1–3]. This process is used to maintain farming production for 40% of the Earth's population, however, it has caused serious pollution problems via large emission of greenhouse gases to the atmosphere constantly [4]. Therefore, looking for a new high energy efficiency method for

* Author to whom any correspondence should be addressed.

nitrogen fixation complementing the Haber-Bosch process is of crucial importance [1]. Plasma-based N-fixation is considered to be a promising candidate where NO formation happens as a result of N_2 and O_2 dissociation via so called Zeldovich mechanism [5–7], involving vibrationally excited states of N_2 and O_2 ($N_2(v) + O \rightarrow NO + N$, $O_2(v) + N \rightarrow NO + O$). In order to enhance the fixation efficiency, additional plasma-chemical processes such as combination plasma with catalyst (e.g. Al_2O_3), were also proposed [8]. Various plasma reactors with different configurations, have been developed for NO production with air as raw materials, including spark discharge [9], glow discharge [10–12], sliding arc and dielectric barrier discharge (DBD) [13–15], etc.

As compared to the low-temperature (or 'cold') plasma sources, such as DBD, where gas temperature (T_g) is about hundreds Kelvin, 'warm' plasmas such as glow or arc-type discharges, where T_g may be as high as thousand(s) Kelvin [16–18], tend to facilitate nitrogen fixation and show higher energy efficiency of this process [11, 19]. From a theoretical point, the energy cost limit of N-fixation by plasma synthesis is more than 2.5 times lower than the value of 30 GJ/tN (gigajoules per metric ton nitrogen produced) of the HB [20], however, the reported energy costs are still no lower than 100 GJ/tN [21]. For profound understanding of the plasma processes responsible for NO formation, a precise *in situ* monitoring of the produced NO compound is of significant importance, from points of both the fundamental research and practical application. Obviously, this will lead to a further insight of the space-resolved energy cost by the N-fixation process in the plasma source, which is critical for the improvement of the nitrogen fixation technology via further fundamental investigations.

In situ measurements of NO molecule in plasma sources are rare, particularly for high (atmospheric) pressure warm air discharges. This is dominantly ascribed to the complicated analysis of detected signal, for example by the method of laser-induced fluorescence (LIF) spectroscopy, for the purpose of absolute quantification [22–24]. Under atmospheric or higher gas pressures, the competitions between the fast energy transfer processes (time scale of ps to ns), including collisional quenching, rotational and vibrational transitions, result in a complicated LIF process difficult to quantify NO density precisely [24, 25]. On the other side, methods by absorption spectroscopy are not suffering from above fast energy transfer processes, and are proper ways for absolutely determining the NO production in plasmas under high pressures [26, 27]. Since intensive absorption of NO molecule locates in the Mid-infrared range, proper light sources for instance the Mid-infrared quantum cascade laser (QCL), are required [27, 28]. Up to now, absolute NO density measurements by QCL absorption spectroscopy (QCL-AS) in high-pressure plasmas are further rare, and only the work by M Simeni *et al* has reported quantitative monitoring of NO density in a 'cold' atmospheric-pressure nanosecond repetitively pulsed air plasma [29]. *In situ* quantification of NO production in 'warm' air discharges at atmospheric (or higher) pressure, has still been absent.

In this work, *in situ* spatial measurements of NO synthesis were presented for the first time along a pin-pin type warm air glow discharge by the approach of Mid-infrared QCL-AS. The selection of pin-pin type DC-driven air glow discharge in this work, is due to its stable property facilitating optical diagnostics, and its potentially high energy efficiency of nitrogen fixation [30]. Sensitive method of wavelength modulation spectroscopy (WMS) was implemented to enhance the signal/noise (S/N) level of QCL-AS measurements. Based on that, energy efficiency of NO generation in different discharge zones of this typical warm plasma reactor was obtained and analyzed, under various conditions of airflow rates and discharge currents.

2. Experimental setup

2.1. The warm air glow discharge

The air glow discharge setup is shown schematically in figure 1. The pin-pin electrodes (diameters of 1.6 mm and 6 mm) are fixed coaxially inside a cross-type cylindrical Pyrex glass tube (with same inner and outer diameters of 10 mm and 14 mm, lengths of 20 mm and 60 mm, respectively). Two CaF_2 windows are attached parallelly on both sides of the horizontal tube for the transmission of Mid-IR laser beam. The two electrodes are conductively fastened by aluminum holders, where the bottom grounded one was movable vertically by the help of a micrometer. Plasma was firstly generated through ignition of a small electrode gap around 0.2 mm, and then was lengthened to 5 mm. A ballast 50 kΩ resistor is used between the upper electrode and a DC power supply to limit the flowing current in the circuit to avoid arc discharge transition. Dry airflow from the bottom to the top was applied in a flow range of 0.5 to 5.0 slm.

2.2. WMS-based QCL-AS system

A thermoelectrically cooled Mid-infrared QCL (L12005-1900H-C, Hamamatsu) operating at 5.2 μm was applied for the NO quantification. The operation temperature and current of the laser chip were stabilized and controlled precisely by two high precision temperature and current controllers (TC5 LAB and QCL1500 LAB, Wavelength Electronics). The Mid-infrared light was firstly collimated to a round beam with diameter of 8 mm, and then reshaped to a thin laser sheet with a scale of 0.5 × 8 mm^2 by a slit, as illustrated in figure 1. The wide Mid-infrared laser sheet passed transversely through the air glow discharge column and refocused by a CaF_2 lens, after that collected by a cooled IR detector (PVI-4TE, VIGO System). A long-pass filter (FELH1500, Thorlabs) was attached in front of the IR detector to remove the radiation interference from the air discharge. It should be pointed out that the utilization of a wide laser sheet but not a focused laser beam in the QCL-AS measurements, is to increase the S/N level. Since the plasma column was almost covered fully by the laser sheet in the radial *XY* plane, space-averaged NO production in this transverse *XY* plane was probed and in this way axially resolved NO population was obtainable along the whole discharge column (*Z*-axis), by moving the setup vertically.

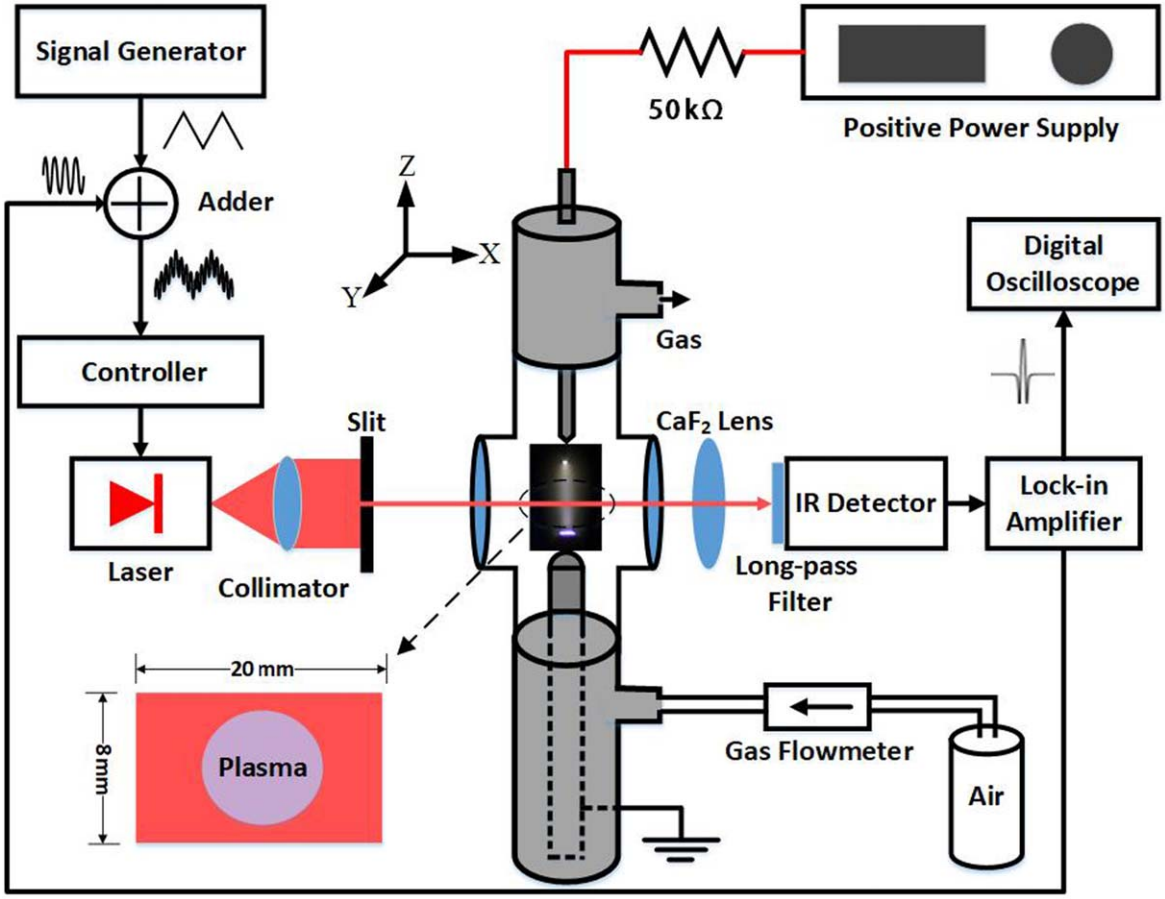

Figure 1. Schematic of the experimental setup including the warm air glow discharge device and the Mid-infrared QCL-AS system with the WMS unit.

The WMS method was applied to enhance the detection sensitivity of QCL-AS due to weak signal of direct absorption through the Beer–Lambert Law, even by using a wide laser sheet. WMS is based on the modulation (normally in range of kHz to MHz) of the laser light that is simultaneously tuned slowly through the absorption profile of the probed species [28, 31–33]. The modulation was driven by a sinusoidal wave at 10 kHz frequency and V_{pp} of 16 mV generated by a lock-in amplifier (SR830, SRS), and superimposed upon a ramp voltage of ±30 mV at frequency of 5 Hz from a signal generator (AFG2021, Tektronix). The laser wavelength was scanned by this ramp voltage of a tuning range covering the absorption line profile of NO. The superimposed ramp signal was then added to the current controller, and in this way the intensity and wavelength of the laser were modulated simultaneously. The optical signal detected by the IR detector was finally collected by the lock-in amplifier, therein the interaction of the modulated light and the absorption spectrum leads to generation of signals at different harmonics of the modulation frequency f. Here the second harmonic signal WMS-2f was demodulated by the lock-in amplifier and recorded by a digital oscilloscope (DPO3000, Tektronix).

In this work, two ro-vibrational transitions between the vibrational levels $v = 0$ and $v = 1$ in the NO($X^2\Pi$) ground-state, namely the $(X_{0.5}, v = 0) \rightarrow (X_{0.5}, v = 1)$ at 1900.076 cm^{-1} (line 1) and the $(X_{1.5}, v = 0) \rightarrow (X_{1.5}, v = 1)$ at 1900.517 cm^{-1} (line 2), were selected in the WMS-based absorption measurements. As illustrated in figure 2, the S/N level is apparently enhanced by the WMS-2f (peak-to-peak) compared to the direct absorption one, under the same gas condition of NO mixture flowing through a 20 mm long absorption cell.

3. Analysis of WMS signal for NO quantification

The peak-to-peak value S_{2f}, as illustrated in figure 2(b), correlates to the NO population on the laser path by the following formula [28, 32]:

$$S_{2f} = -\frac{G\bar{I}_0}{2} PxS^*LH_2 \quad (1)$$

In above formula, G represents the optical–electrical gain of the WMS-2f detection system and calibrated through measurements of reference gas with known NO density. $\bar{I}_0$ is the averaged laser intensity detected when the plasma is off, P is the gas pressure (1 atm here), x is the molar volume fraction of NO, and L is the absorption length of 20 mm here. S^* is the pressure-corrected line strength (unit: cm^{-2}/atm), and H_2 is the second harmonic component. The detailed calculations of the two parameters are described as below [34].

$$S^* = 7.34 \times 10^{21} \frac{S_{T_g}}{T_g} \quad (2)$$

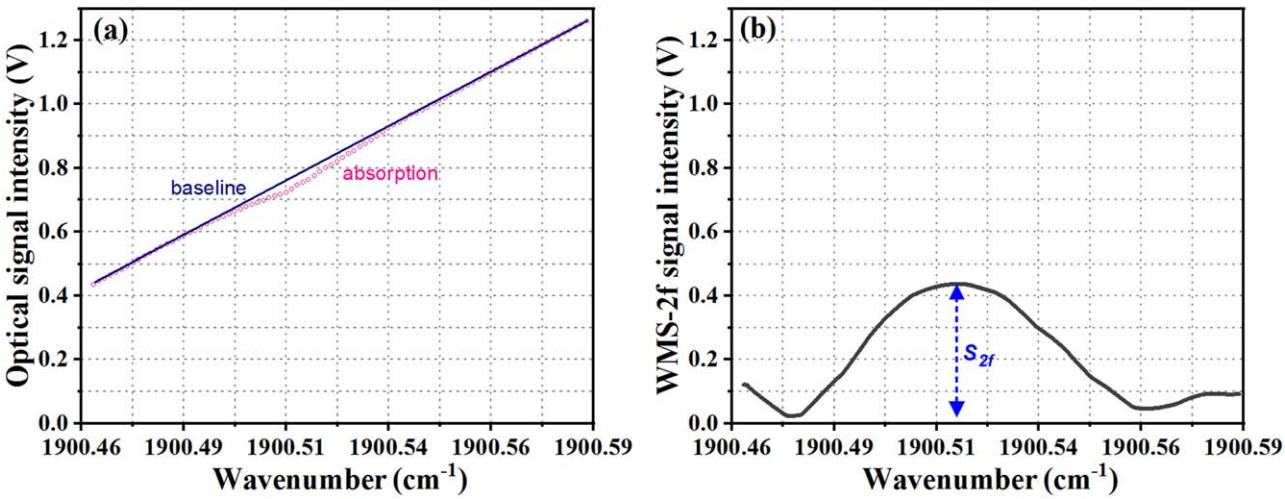

Figure 2. Profiles of (a) direct absorption spectrum and (b) WMS-2*f* signal of the 1900.076 cm^{-1} absorption line (line 1) of NO, under the same gas condition of N_2 + 0.4%NO at a flow rate of 2.0 slm through a 20 mm long absorption cell.

where S_{T_g} is the spectral line strength (unit: cm^{-1}/molecule·cm^{-2}) and only dependent on the gas temperature T_g. S_{T_g} can be calculated under different gas temperatures, through the following formula [34]:

$$S_{T_g} = S_{T_{ref}} \frac{Q_{T_{ref}}}{Q_{T_g}} \cdot \frac{1 - \exp\left(-\frac{hcv_0}{kT_g}\right)}{1 - \exp\left(-\frac{hcv_0}{kT_{ref}}\right)} \cdot \exp\left[-\frac{hcE_l}{k}\left(\frac{1}{T_g} - \frac{1}{T_{ref}}\right)\right] \quad (3)$$

where Q_{T_g} is the total internal partition function and dependent on the gas temperature T_g, E_l is the energy of the lower level of selected absorption transition, h, c, k, v_0 are Plank constant, light speed, Boltzmann constant, and the center frequency of the spectral absorption line, respectively. The subscript ref represents parameters calculated under room temperature T_{ref} = 296 K. The total internal partition function Q_{T_g} is given by:

$$Q_{T_g} = \sum_k g_k \exp\left(-\frac{hcE_k}{kT_g}\right) \quad (4)$$

where g_k is the statistical weight of the k-level with energy E_k. All above parameters, including the reference values $S_{T_{ref}}$, can be found in the HITRAN database [34]. Therefore, the values of Q_{T_g} and then S_{T_g}, and finally the S^* under different T_g are obtainable based on above formula [28, 29, 32].

The second harmonic component H_2 is calculated by [32]:

$$H_2 = \frac{1}{\pi}\int_{-\pi}^{\pi} \varphi(v)\cos(2\theta)\mathrm{d}\theta \quad (5)$$

where $\varphi(v)$ is the line-shape function of the NO absorption line, and dependent on the gas temperature T_g. The detailed calculation of $\varphi(v)$ is referred to the HITRAN database [34].

Therefore, the values of both the S^* and H_2 are calculable under different T_g for the two NO absorption lines, and the ratios of $\frac{S^*_{(1)} \cdot H_{2(1)}}{S^*_{(2)} \cdot H_{2(2)}}$ are obtainable for different T_g, as depicted in figure 3. The curve in figure 3 was then applied to calibrate the space-averaged $\bar{T}_g$ over the probed radial cross section of the air glow discharge column, by the following formula [31]:

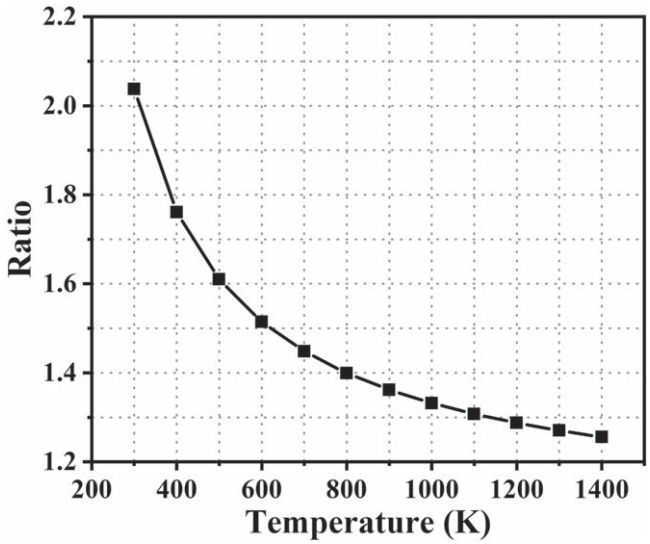

Figure 3. The ratio of $\frac{S^*_{(1)} \cdot H_{2(1)}}{S^*_{(2)} \cdot H_{2(2)}}$ of the two NO absorption lines as a function of gas temperature.

$$ratio = \frac{S_{2f(1)} \cdot \bar{I}_{0(2)}}{S_{2f(2)} \cdot \bar{I}_{0(1)}} = \frac{S^*_{(1)} \cdot H_{2(1)}}{S^*_{(2)} \cdot H_{2(2)}} \quad (6)$$

In calibration measurements, pure NO gas (99.99% purity) was mixed with N_2 background gas at a ratio range of 0.2% to 0.8%, at room temperature and 1 bar pressure. The reference gases of different NO% were flowing through an absorption cell consisting of a gas tube (length of 20 mm, inner diameter of 10 mm) with two CaF_2 windows attached at two ends. Figure 4 presents the measured spectral profiles of WMS-2*f* signals of line 1, and corresponding linear dependency of the S_{2f} value on the value of $\left(\frac{\bar{I}_0}{2}PxS^*LH_2\right)$ as described in above equation (1). From that, the G value was determined and

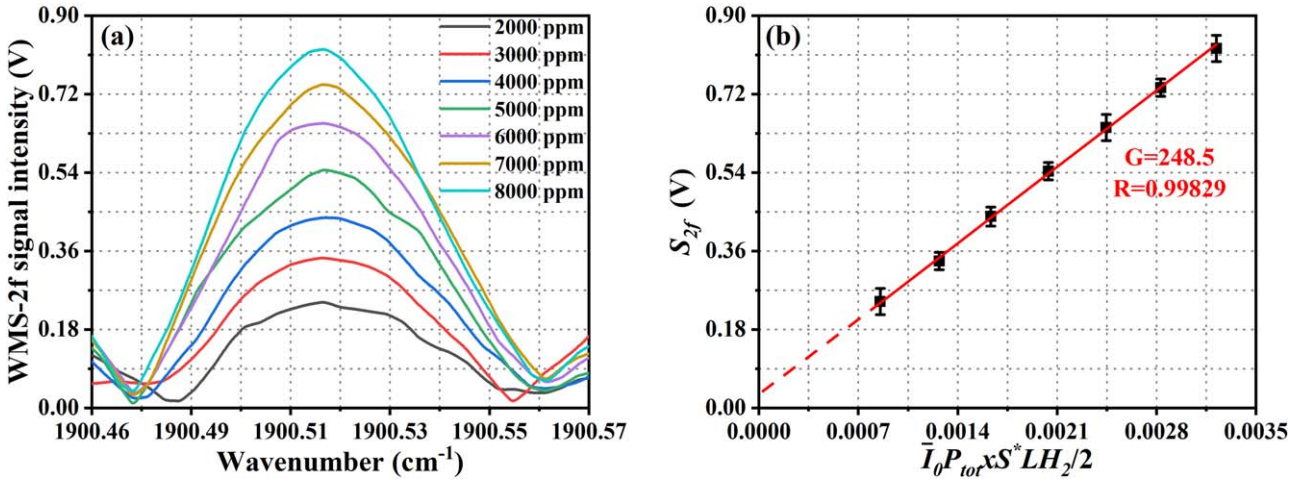

Figure 4. (a) Detected spectral profiles of WMS-2*f* signal of line 1 and (b) linear fitting curve of S_{2f} value upon the value of $\left(\frac{\bar{I}_0}{2}PxS^*LH_2\right)$, under different NO ratios in the NO/N_2 reference gas at room temperature and 1 bar pressure.

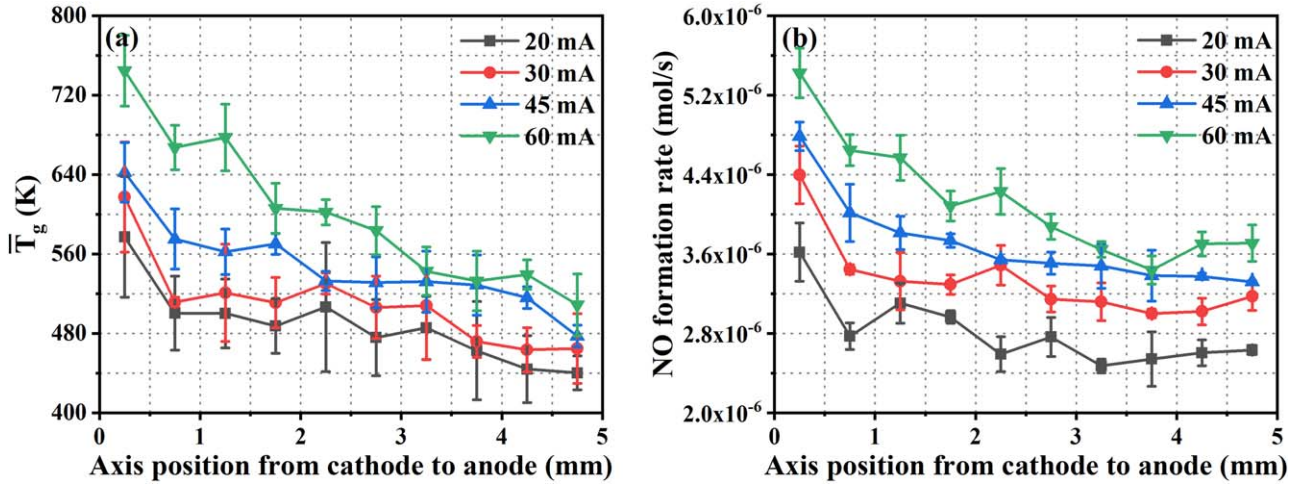

Figure 5. The axially resolved distributions of (a) radially averaged gas temperature $\bar{T}_g$ and (b) NO synthesis rate under different discharge currents, and airflow rate of 1.0 slm.

applied to the WMS absorption measurements of NO in the studied air glow discharge under different conditions. It should mention that, all the WMS-based QCL-AS measurements were performed after 10-min operation of the air discharge. The discharge was expected to achieve kinetic equilibrium state during the QCL-AS measurements, including the gas flow field and plasma properties.

4. Results and discussion

4.1. Effects of current and airflow rate

The impacts of discharge current and air gas flow on the radially averaged NO productions and $\bar{T}_g$ along the discharge column, are presented in figures 5 and 6. As observed that, with increase of the discharge current, the NO synthesis at each plasma region along the discharge column rises. Similar trends of averaged gas temperature $\bar{T}_g$ are observed as well upon the discharge current. This is as expected due to more electrical energy dissipated by plasma with rise of current. It is interesting to show that along the plasma column, a steep rise is observed for both the NO production and $\bar{T}_g$ while approaching to the cathode region, as depicted in figure 5. Higher gas temperature in the hotter cathode region is expected, due to the sharp voltage drop and high energy density deposited in the thin cathode sheath (typically less than 10^2 μm at atmospheric pressure) [35, 36]. Intense discharge as a result of dense deposition of electrical energy in the thin cathode region, leads to higher gas temperature and higher generation of NO therein.

A similar tendency is observed for the NO generation with rise of the airflow rate, as shown in figure 6. The local synthesis rates of NO along the whole discharge column raise while the airflow rates increase from 0.5 to 2.0 slm. Whereas, a slight decline of the averaged $\bar{T}_g$ is expected due to the enhanced cooling effect with rise of the airflow.

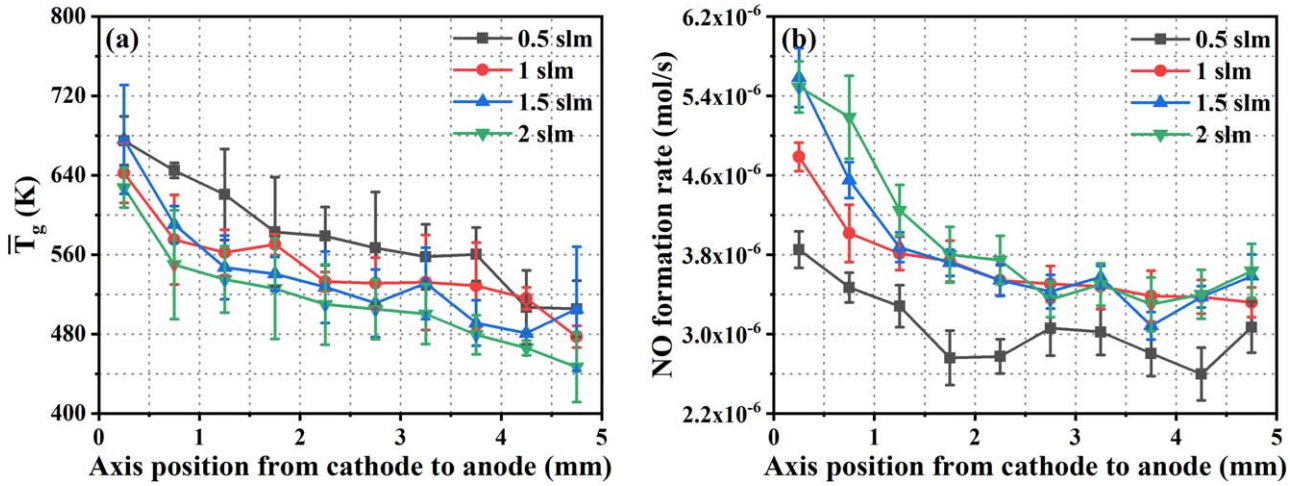

Figure 6. The axially resolved distributions of (a) radially averaged gas temperature $\bar{T}_g$ and (b) NO synthesis rate under different airflow rates, and discharge current of 45 mA.

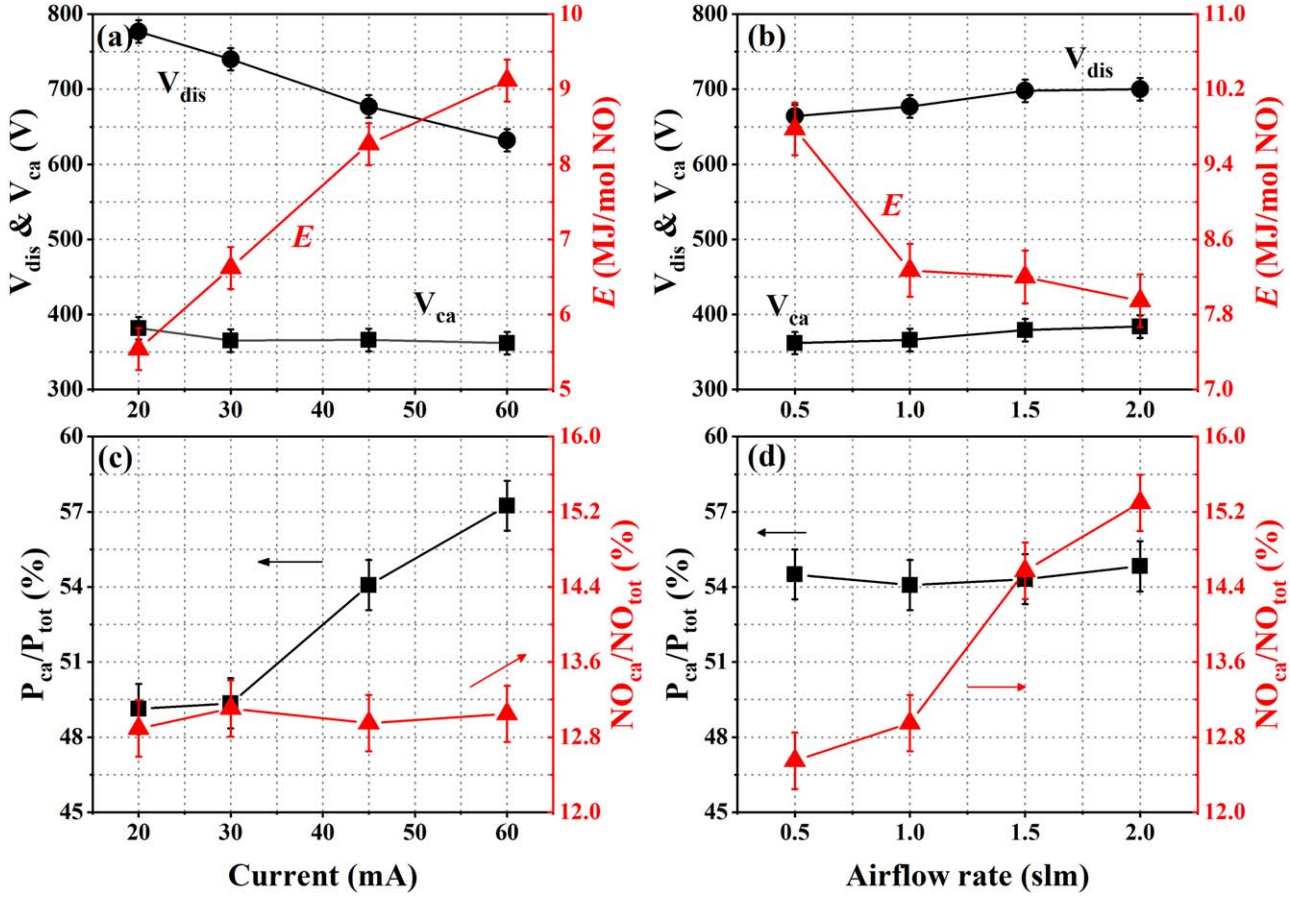

Figure 7. (a) and (b) The measured voltages applied to the whole discharge column V_{dis} and the cathode sheath V_{ca}, energy efficiency E. (c) and (d) Ratios of power dissipation and NO synthesis by the cathode region over the whole discharge, under different currents or airflow rates.

4.2. Energy efficiency of NO synthesis in cathode and non-cathode regions

The corresponding energy efficiency E of NO synthesis under above discharge conditions is illustrated in figure 7. The energy efficiency E over the whole discharge zone is calculated by:

$$E = \frac{P_{dis} \times 60}{\frac{f}{V} \times c_{NO} \times 10^{-6}} \times 10^{-6}\ (\mathrm{MJ\ mol^{-1}\ NO}) \qquad (7)$$

Here, P_{dis} is the electrical power consumption (W) dissipated

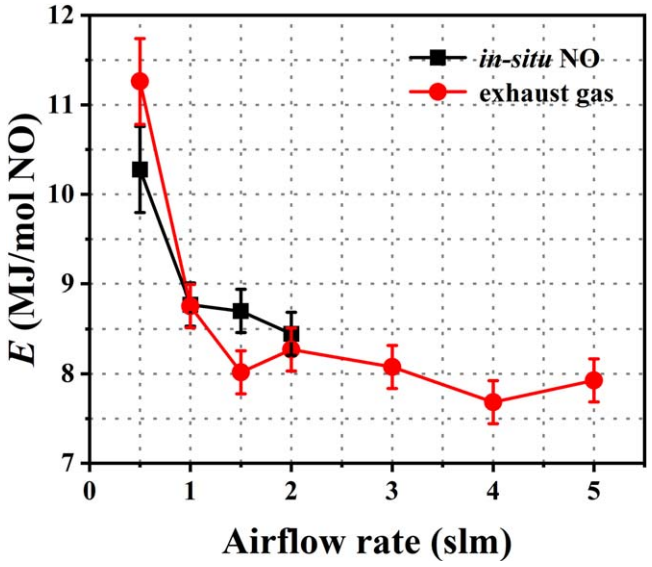

Figure 8. Energy efficiency E of NO synthesis by the air glow discharge determined based on *in situ* monitored NO productions therein, and its exhaust gas upon airflow rate (from 0.5 to 2.0 slm).

by the whole air discharge, f is the airflow rate (l min^{-1}), c_{NO} is the volume fraction of NO (ppm), V (l mol^{-1}) is the molar volume of ideal gas at 1.0 bar pressure and dependent on gas temperature. Here the volume-averaged $\bar{T}_g$ over the whole discharge chamber ($\pi \times 5.0^2 \times 20$ mm^3) was used and calculated by averaging the axially resolved $\bar{T}_g$ along the plasma column. The factor of 10^{-6} in the numerator arises from the unit conversion of J mol^{-1} to MJ mol^{-1}.

As shown in figure 7(a), the energy cost of NO production raises at high discharge currents. Although the NO synthesis rate increases with rise of current, as presented in figure 5, its increase rate is much slowly compared to that of consumed electrical power upon the discharge current, as shown in figure 7(c). An opposite trend was observed that, the energy cost of NO synthesis reduces by increasing the airflow rate applied to the discharge, as shown in figure 7(b). A drop of E value from 9.8 to 8.0 MJ mol^{-1} was achieved while the airflow rate increases from 0.5 to 2.0 slm. Further decline of E is expected if larger airflow rate is applied, as proved by detections of NO density in the exhaust gas of the air discharge reactor, and illustrated in figure 8. The S/N level of WMS absorption passing through the discharge is too low to be detectable at higher airflow rates than 2.0 slm. Therefore, NO measurements were performed as well for the exhaust gas of the air discharge by the same WMS absorption as above, except that the absorption length was increased to 40 mm by using another absorption cell consisting of a gas tube (length of 40 mm, and inner diameter of 10 mm). The gas tube, attached by two CaF_2 windows at two ends, was connected to the gas output of the discharge reactor by another flexible gas pipe (length of 100 mm). The comparable E levels of the air glow discharge determined based on *in situ* NO productions therein and its exhaust gas upon airflow rate (from 0.5 to 2.0 slm), as presented respectively in figure 8, demonstrate the validity of the implemented WMS-based QCL-AS for *in situ* probing NO synthesis along this warm air plasma source. As can be seen, a saturation level of E tends to be achieved if further increasing the airflow rate, which indicates limitation of large airflow on further improving the energy efficiency of NO synthesis in this air discharge. Similar phenomena have been reported in other warm air discharges, including glow-like or arc-like plasma sources [8]. These limitations by the control of discharge operation conditions, including current, airflow rate, or even electrode gap [11, 14], imply that other improvement actions able to enhance the formation process of NO selectively, are desired.

The voltage drop of the cathode region V_{ca} was measured under above discharge conditions, by extrapolating the linear curves of the applied voltage as a function of the inter-electrode distance to zero [37]. The measured voltages V_{dis} applied to the whole discharge gap under different conditions, are presented in figure S1. The corresponding levels of the V_{ca} were obtained from these linear V_{dis} curves extrapolated to zero. Almost half of discharge voltage, namely half of electrical power, is deposited in this thin cathode sheath, as shown in figures 7(c)–(d). However, from the *in situ* measurements of NO productions, the cathode region contributes disproportionally ranging only from 12% to 16% to the NO synthesis by the whole discharge. This is costly in consuming electrical energy and finally drags down the energy efficiency level of the whole warm air discharge source, for the purpose of nitrogen fixation. This power ratio by the cathode sheath can be reduced to around 20% if the electrode gap was extended to 20 mm under 30 mA, however, the corresponding contribution of NO synthesis drops to be less than 3% (measured by the same WMS absorption procedure as above, data are not shown here). Further increase of the electrode gap larger than 20 mm requires higher currents to sustain the discharge, which means higher consumption of electrical energy but not lower E level [8].

The high energy cost of NO synthesis in the cathode region ascribes dominantly to the energy transfer process not selectively preferable for the formation of NO therein. The reduced electric field E/N in the region close to the cathode electrode, with a thickness of 0.5 mm same to that of laser sheet, was estimated from the measured V_{ca} and $\bar{T}_g$. A uniform electric filed crossing this region was assumed and calculated directly by $E_{ca} = V_{ca}/d_{ca}$. The corresponding radial distribution of gas temperature $T_g(r)$ was deduced from the measured $\bar{T}_g$ by assuming a symmetric Gaussian distribution. This symmetric assumption of $T_g(r)$ is reasonable and has been proved in our previous work by the method of calibrated Schlieren photograph [36, 38]. A peak of T_g around 3300 K was estimated in this cathode-nearby region, if $T_g(r)$ with a full-width at half maximum (FWHM) of 2 mm, under the current of 20 mA and airflow of 1.0 slm. This T_g peak increases to 4500 K if the current rises to 60 mA. By that, radial distributions of E/N in the cathode-nearby region were calculated, based on the ideal gas law $P = NkT_g$, with k the Boltzmann constant. Extremely high E/N level was estimated with more than 50% proportions larger than 100 Td, under the condition of 20 mA and 1.0 slm. This E/N magnitude is expected to be underestimated for the true cathode sheath due to its thin thickness less than 10^2 μm at high gas

pressure [31], but not 0.5 mm used in above estimation. Furthermore, the real gas temperature in the cathode sheath is expected to be higher than the estimated one above [36, 39], which leads to a smaller air density N and finally again results in a much higher E/N therein. The extremely strong reduced electric field in the cathode sheath, stimulates productions of energetic electrons inducing processes of electronic excitations and ionizations significantly, but not selectively preferable for processes of vibrational excitations or dissociations of N_2 and O_2 molecules which require E/N lower than 100 Td [11, 14, 19]. The latter two electron energy transfer processes are crucial for the formation of NO molecule through the Zeldovich reactions $N_2(v) + O \rightarrow NO + N$ and $O_2(v) + N \rightarrow NO + O$ [5, 9, 21]. That means in the cathode region, the selectivity of energy transfer to the Zeldovich reactions, namely the processes of vibrational excitations or dissociations of N_2 and O_2 molecules, are low due to extremely high E/N therein. This finally induces a very low energy efficiency of NO synthesis in the cathode area of the air glow discharge.

For the main part of the air glow discharge, which is dominated by the positive column (P.C.) region, the estimated E/N level therein drops drastically below 60 Td, as estimated in a same way to that of the cathode region. This low E/N level facilitates the vibrational excitation processes of N_2 and O_2 molecules, and promotes the synthesis of NO in the PC zone with a much higher energy efficiency compared to that of the cathode region. However, as presented above, further reduction of the energy cost of NO production is actually ineffective through variations of the operational conditions, including current or airflow, of this air glow discharge. This probably be ascribed to the unapparent variation of E/N levels in the long PC region upon the change of these operation conditions. It implies that other actions, such as ways able to tune the E/N levels in the discharge and selectively deliver energy to the Zeldovich process of NO formation, and to suppress the loss process of NO, etc, are desired to further optimize the energy efficiency of NO synthesis by this warm air discharge [19]. And based on the results in this work, decrease of the energy cost in the cathode region will promote the NO synthesis in a more efficient way, particularly for warm air plasmas with short electrode gaps.

5. Conclusions

In this work, the production of NO as an important product of plasma-based nitrogen fixation, was quantified *in situ* in a typical warm air glow discharge by the technology of WMS-based Mid-infrared quantum cascade laser absorption spectroscopy (QCL-AS). The results demonstrate that, although higher synthesis rate of NO was found for the region of thin cathode region, much lower energy efficiency was found disproportionately, compared to that of the positive column of the main discharge zone. Further analysis by the estimation of the reduced electric filed E/N, indicates that the energy-intensive NO production is resulted by the extreme high E/N ratio in the cathode region, wherein electronic excitations and ionizations occur dominantly but not vibrational excitations or dissociations of N_2 and O_2 molecules. Furthermore, the unapparent tune of E/N levels in the main discharge column, implies limitations of further optimizing the energy efficiency of NO synthesis by simply controlling the operational conditions of the used air glow discharge. Other manners able to optimize the energy transfer selectively to the Zeldovich process, such as reducing the energy cost in the cathode area by for example efficient cooling of the hot cathode area, are of practical importance for improving the warm air-discharge-based NO synthesis process in the future.

Acknowledgments

This work was partly supported by National Natural Science Foundation of China (Nos. 11975061, 52111530088), the Technology Innovation and Application Development Project of Chongqing (No. cstc2019jscx-msxmX0041), the Construction Committee Project of Chongqing (No. 2018-1-3-6), and the Fundamental Research Funds for the Central Universities (No. 2019CDQYDQ034). We also appreciate Dr Nikolay Britun (Center for Low-temperature Plasma Sciences, Nagoya University, Japan) for the helpful discussions.

References

[1] Chen J G *et al* 2018 *Science* **360** eaar6611
[2] Cherkasov N, Ibhadon A O and Fitzpatrick P 2015 *Chem. Eng. Process.: Process Intensific.* **90** 24
[3] Tanabe Y and Nishibayashi Y 2013 *Coord. Chem. Rev.* **257** 2551
[4] Erisman J W *et al* 2008 *Nat. Geosci.* **1** 636
[5] Fridman A 2008 *Plasma Chemistry* (Cambridge: Cambridge University Press)
[6] Graves D B *et al* 2019 *Plasma Chem. Plasma Process* **39** 1
[7] Ingels R and Graves D B 2016 *Plasma Med.* **5** 257
[8] Pei X K, Gidon D and Graves D B 2020 *J. Phys. D: Appl. Phys.* **53** 044002
[9] Britun N, Gamaleev V and Hori M 2021 *Plasma Sources Sci. Technol.* **30** 08LT02
[10] Pei X K, Gidon D and Graves D B 2018 *Plasma Sources Sci. Technol.* **27** 125007
[11] Pei X K *et al* 2019 *Chem. Eng. J.* **362** 217
[12] Zhu Y *et al* 2021 *Plasma Process. Polym.* **18** 2000223
[13] Chen H *et al* 2021 *Plasma Process. Polym.* **18** 2000200
[14] Jardali F *et al* 2021 *Green Chem.* **23** 1748
[15] Patil B S *et al* 2016 *Appl. Catal. B: Environ.* **194** 123
[16] Adams S F, Caplinger J E and Sommers B S 2015 *Plasma Sources Sci. Technol.* **24** 025031
[17] Sommers B S and Adams S F 2015 *J. Phys. D: Appl. Phys.* **48** 485202
[18] Verreycken T *et al* 2010 *Plasma Sources Sci. Technol.* **19** 045004
[19] Wang W Z *et al* 2017 *ChemSusChem* **10** 2145
[20] Rusanov V D, Fridman A A and Sholin G V 1981 *Sov. Phys. Usp.* **24** 447
[21] Rouwenhorst K H R *et al* 2021 *Energy Environ. Sci.* **14** 2520
[22] Burnette D *et al* 2016 *Plasma Sources Sci. Technol.* **25** 025012
[23] Van Gessel A F H *et al* 2013 *J. Phys. D: Appl. Phys.* **46** 095201
[24] Preissing P *et al* 2020 *Plasma Sources Sci. Technol.* **29** 125001

[25] Van Gessel A F H and Bruggeman P J 2013 *J. Chem. Phys.* **138** 204306
[26] Reuter S *et al* 2015 *Plasma Sources Sci. Technol.* **24** 054001
[27] Welzel S *et al* 2010 *Sensors* **10** 6861
[28] Sun K *et al* 2013 *Meas. Sci. Technol.* **24** 125203
[29] Simeni M S, Laux C O and Stancu G D 2017 *J. Phys. D: Appl. Phys.* **50** 274004
[30] Kelly S and Bogaerts A 2021 *Joule* **5** 3006
[31] Rieker G B, Jeffries J B and Hanson R K 2009 *Appl. Opt.* **48** 5546
[32] Peng Z M *et al* 2011 *Opt. Express* **19** 23104
[33] Tachibana K *et al* 2018 *Jpn. J. Appl. Phys.* **57** 0102BB
[34] HITRAN online, Definitions and Units: Line-by-line Parameters (https://hitran.org/docs/definitions-and-units/)
[35] Bruggeman P J, Iza F and Brandenburg R 2017 *Plasma Sources Sci. Technol.* **26** 123002
[36] Xiong Q *et al* 2018 *J. Phys. D: Appl. Phys.* **51** 095207
[37] Bruggeman P *et al* 2008 *J. Phys. D: Appl. Phys.* **41** 215201
[38] Xiong Q *et al* 2018 *Plasma Sources Sci. Technol.* **27** 095010
[39] Mezei P, Cserfalvi T and Csillag L 2005 *J. Phys. D: Appl. Phys.* **38** 2804